JACS
JOURNAL OF THE AMERICAN CHEMICAL SOCIETY

Article

pubs.acs.org/JACS

Evidence for Core Oxygen Dynamics and Exchange in Metal Oxide Nanocrystals from In Situ ^{17}O MAS NMR

Yohan Champouret, Yannick Coppel,* and Myrtil L. Kahn*

Laboratoire de Chimie de Coordination du CNRS, 205 route de Narbonne, 31077 Toulouse Cedex 04, France

Supporting Information

ABSTRACT: Long-term stability of the properties of nanocrystals (NCs) is of paramount importance for any applicative development. However, these are jeopardized by chemical and structural alterations of the NCs induced by the environment and the working conditions. Among the species that alter the NCs properties, water molecules are of tremendous importance. We used ^{17}O solid-state NMR spectroscopy to follow this process and the dynamics of O atoms in metal oxide NCs. Using ZnO as reference material, different chemical environments for the O atoms are characterized and a dynamic exchange process between the NCs and the O atoms from water is evidenced. The exchange does not involve only surface atoms but also ones located deeper inside the ZnO core of the NCs. Finally, a postsynthesis process based on watering/drying cycles is proposed that may greatly improve the long-term stability of metal oxide NCs.

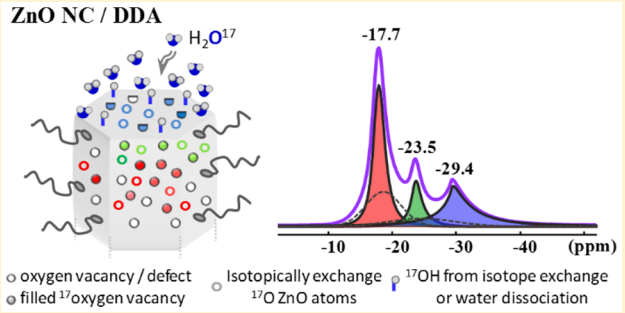

INTRODUCTION

Whether nanocrystals (NCs) are designed to be implemented into microelectronic devices or used for their reactivity (e.g., in catalysis or for sensors), long-term stability of their properties is of paramount importance. However, these are jeopardized by chemical and structural alterations of the NCs induced by the environment and the working conditions.[1−4] This encompasses surface reactivity of the NCs but also possible reorganization of the core atoms themselves. Probing the motion of atoms constitutive of a NC, as well as their dynamics in connection with the particle's reactivity with the environment, remains a challenging issue. We show herein that solid-state MAS NMR spectroscopy, which is classically used to investigate the composition and the local structure in various NC systems,[5−7] may also be suited to address this challenge and allows for probing the migration and dynamic characteristics of the core atoms.

Among the most typical species present in ambient working conditions, water molecules are known to often significantly alter the NCs properties.[1−4] We used ^{17}O solid-state NMR[8−11] to follow this process and the dynamics of O atoms in metal oxide NCs. Using ZnO—an n-type semiconductor with physical (conduction, optical properties) and chemical properties of particular interest[12−15]—as reference material, different chemical environments for the O atoms are characterized and a dynamic exchange process between the NCs and the O atoms from water is evidenced. The exchange involves not only surface atoms but also ones located deeper inside the ZnO core of the NCs. Moreover, we show that the exchange kinetics are dependent on the shape of the NCs.

To date, very few ^{17}O solid-state NMR spectra of ZnO have been reported, all showing a single resonance at −18 ppm.[16−18] To obtain ^{17}O NMR spectra of good quality, isotopic enrichment is necessary. This was achieved by taking advantage of the known dissociation process of H_2O molecules at the surface of ZnO.[19−22] Exposing the NCs to ^{17}O-enriched H_2O resulted in O exchange between the water and the metal oxide yielding ^{17}O-enriched ZnO; this exchange process was monitored by in situ NMR experiments.

RESULTS AND DISCUSSION

Two different morphologies of NCs were considered (Figure 1 and Figure S1): (i) isotropic NCs (sample 1, mean size 5.6 ± 1.2 nm) and (ii) nanorods (sample 2, width = 5.4 ± 0.8 nm,

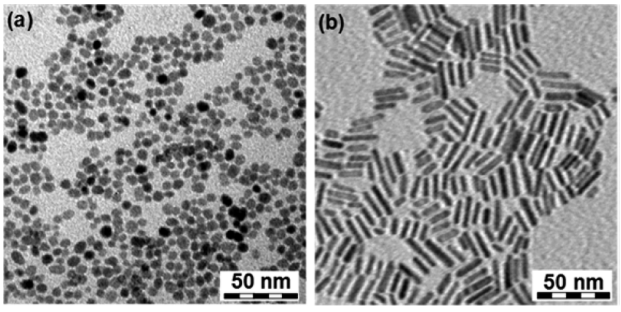

Figure 1. TEM images of (a) isotropic NCs (sample 1) and (b) nanorods (sample 2).

Received: August 26, 2016
Published: November 24, 2016

DOI: 10.1021/jacs.6b08769
J. Am. Chem. Soc. 2016, 138, 16322−16328

length = 15.8 ± 8.5 nm). For a matter of comparison (vide infra), the width of the rods is equal to the mean diameter of the isotropic NCs. These samples were synthesized by a controlled hydrolysis of $[Zn(Cy)_2]$ (Cy stands for cyclohexyl) in the presence of dodecylamine (DDA) either in a tetrahydrofuran (THF) solution (sample 1) or in pure amine (sample 2).[23] A washing procedure was applied to remove the excess of ligand, but the surfaces for both NCs are still stabilized by strongly bound amine ligands (Figure S2). Previous studies proved that the isotropic NCs are nanohexagons of aspect ratio close to 1[24] with the amine ligands bound only to the lateral faces (i.e., [10−10] and [1−100] planes), not on the basal ones (i.e., [0001] plane).[25,26]

In a typical NMR experiment, 20 μL of H_2O enriched in ^{17}O (enrichment degree of 20%) was added (under an argon gas stream) to a dry ZnO NC sample (ca. 30 mg) loaded in the MAS rotor. O exchange in ZnO was investigated following the time dependence of the 1D T_1-filtered ^{17}O MAS NMR spectra (Figure 2 and Figures S3 and S4). Quite sharp ^{17}O resonances

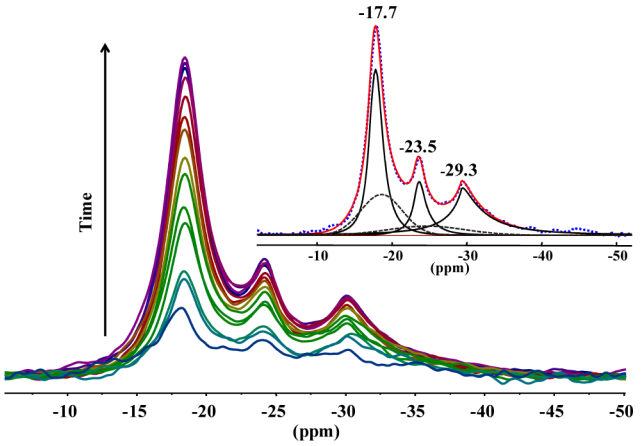

Figure 2. 1D T_1-filtered ^{17}O MAS spectra of nanorods (sample 2) for contact times of 3−26 h with ^{17}O-enriched water. Inset: spectrum after 26 h (in blue) compared to simulated spectrum (in red) with deconvolution (in black). Dashed lines correspond to the spinning sideband contributions of satellite transitions.

with asymmetric shapes characteristic of a distribution of quadrupolar parameters, typical of disordered materials, were observed.[27−30] In such a case, the Czjzek model is well-adapted to simulate the ^{17}O resonances.[27,28,31] Spinning sidebands of the satellite transitions lying underneath the central transitions (Figures S5 and S6) were also taken into account for quantification.[28] The whole ^{17}O ZnO signal can be well-reproduced with three resonances at −17.7(±0.1), −23.5(±0.2) and −29.4(±0.2) ppm (hereinafter called high, medium, and low frequencies, respectively) with average quadrupolar coupling (QC) values of, respectively, 70(±6), 63(±7), and 110(±5) kHz, indicative for O atoms in different chemical surroundings (Figure 2 inset and Figure S7). These weak QC values, which are due to the high ionicity of the Zn−O bond,[8] lead to a favorable situation to distinguish O-sites with different environments. Because of these QC values being of the same order, no other additional correction was performed on the integrated intensities of the central transition.[32]

The ^{17}O enrichment rates, k_{glo} (glo stands for global), were determined by monitoring the changes of the peak integrals for the three ^{17}O ZnO resonances as a function of time according to the expression of the form: $I(t) = I(\infty)[1 - \exp\{-k{\cdot}t\}]$ where $I(t)$ and $I(\infty)$ denote the intensities of the ^{17}O signal for a time t and for the equilibrium state, respectively.[10,33] Note that ^{17}O intensity changes in the T_1-filtered experiment over water contact time (due to possible T_1 relaxation time changes) were considered lower than the error associated with the fitting of the data. It must be emphasized that k_{glo} corresponds to an apparent exchange rate as several phenomena, such as adsorption of the water molecule, its diffusion on the surface, its dissociation, and the diffusion of the O atom, contribute to k_{glo} but cannot be differentiated experimentally. The time dependence of the NMR signal (integral) for the global ^{17}O is plotted in Figure 3, while the evolution for the three individual resonances is given in Figure S8.

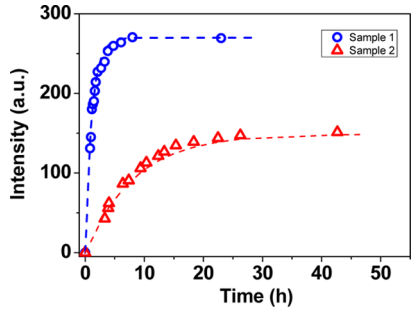

Figure 3. Comparison of the global ^{17}O signal intensities of the isotropic NCs (sample 1, blue empty circle) and the nanorods (sample 2, red empty triangle) as a function of the contact time to enriched H_2O. The fitting curves (---) use the equation $I(t) = I(\infty)[1 - \exp\{-k{\cdot}t\}]$.

The ^{17}O ZnO signal increases right from the beginning of the experiment and within hours reaches a stable value—the final isotope enrichment level (IEL)—indicative of an equilibrium state in the isotope exchanges. Obviously, the ^{17}O exchange is faster for the isotropic NCs than for the nanorods. To allow a sample−oversample comparison, the IEL values given in Table 1 correspond to the maximum value of the global ^{17}O-exchanged ZnO signal integral per milligram of sample. The fitting of the global ^{17}O ZnO signal as a function of time yielded global apparent exchange rate values, k_{glo}, of 0.88 and 0.12 h^{-1}, respectively, for samples 1 and 2, revealing an isotope

Table 1. ^{17}O Apparent Exchange Rates of O Atoms between ^{17}O-Enriched Water and ZnO NCs

sample	k_{glo} [a]	$k_{(high)}$ [a]	$k_{(med)}$ [a]	$k_{(low)}$ [a]	ratio [b]	IEL [c]
1	0.88	0.83	0.88	1.14	82/5/13	270
	(0.02)	(0.02)	(0.05)	(0.03)		
2	0.12	0.10	0.14	0.19	78/7/15	149
	(0.01)	(0.01)	(0.02)	(0.02)		
3	0.14	0.08	0.20	0.48	61/6/33	64
vide infra	(0.01)	(0.01)	(0.02)	(0.03)		
4	0.06	0.06	0.06	0.06	28/23/49	15
vide infra	(0.01)	(0.01)	(0.02)	(0.02)		

[a]Apparent exchange rate (h^{-1}) for the global ^{17}O ZnO signal and for the three individual resonances. [b]Relative population (%) of the three resonances (low/medium/high) found in the equilibrium state by 1D T_1-filtered ^{17}O MAS (with relaxation delay of 20 s). [c]Isotope enrichment level (a.u./mg) obtained by scaling the global area of the ^{17}O ZnO NMR signals in the equilibrium state (Figure S9) to 1 mg of material.

DOI: 10.1021/jacs.6b08769
J. Am. Chem. Soc. 2016, 138, 16322−16328

apparent exchange rate 1 order of magnitude larger for the isotropic NCs. Similar results are obtained regardless of signal considered (i.e., low, medium, and high frequencies; Figure S8) with apparent exchange rates spanning from 0.83 to 1.14 h^{-1} for sample 1 and from 0.10 to 0.19 h^{-1} for sample 2 (Table 1). The apparent exchange rates depend on the surroundings of the O atom. It may also be noticed that the ratio between the three resonances is similar for samples 1 and 2 (Table 1). However, clearly different IELs are found for the isotropic NCs and nanorods (IEL = 270 versus 149). These results indicate that the amount of exchangeable O atoms is related to the size and shape of the NCs but that the concerned O-sites are homogeneously distributed in both samples. Because the DDA ligands are located on the lateral faces of the NCs,[25,26] we can formulate the hypothesis that the basal faces are more accessible to water. This is consistent with the smaller IEL found for the nanorods, for which the relative ratio of basal to lateral planes is 2−3 times smaller than for the isotropic NCs. Indeed, while the basal side surfaces for the hexagons and the rods are the same, the length of the latter corresponds to 2−3 times the diameter, thus proportionally reducing the area of the basal planes per mass unit.

The actual amount of exchangeable O atoms was evaluated by synthesizing isotropic ZnO NCs directly with ^{17}O-enriched (20% enrichment) water (sample 1′, Figure S10) and exposing them to normal water (500 μL, i.e., >100 times more than the oxygen atoms in the ZnO sample) during 4 days. Only two resonances are necessary to simulate the ^{17}O spectrum of sample 1′ before its exposure to normal water (Figure S11). Their chemical shifts, QC values, and population are, respectively, −17.7(±0.1) and −26.5(±0.2) ppm, 77(±5) kHz and 110(±7) kHz, and 80(±3) and 20(±3) %. The high-frequency signals (i.e., at −17.7 ppm) are identical in samples 1 and 1′. For the low-frequency ^{17}O signals, while comparable average quadrupolar coupling is obtained for samples 1 and 1′ (between 60 and 110 kHz for both samples), a much higher isotropic chemical shift distribution is observed for the −26.5 ppm resonance of sample 1′ (11(±1) ppm) than for the medium and low frequencies of sample 1 (<1 ppm). This result suggests that the −26.5 ppm resonance of sample 1′ is a signal characteristic of numerous O environments overlapping at lower frequency (i.e., below the signal at −17.7 ppm). Comparison of the ^{17}O MAS spectra for samples 1 and 1′ also shows that ^{17}O exchange takes place preferentially on specific O sites (Figures 2 and 4a). Indeed, while sample 1′ exhibits only one broad signal observed at −26.5 ppm, two signals are observed at −23.5 and −29.5 ppm for sample 1.

The ^{17}O MAS spectrum of sample 1′ after its exposure to normal water showed a signal loss of 33(±5) % (Figure 4a), well above that for O atoms in the basal faces (ca. 9%; see Supporting Information). Moreover, the −17.7 and −26.5 ppm peaks show a significantly different variation with signal losses of 22(±3) and 50(±5)%, respectively. This demonstrates that only part of the NCs O atoms are exchangeable in the considered experimental conditions, suggests the existence of a stable, inert ZnO core, and substantiates diffusion of O from/to inside the NCs. Such core atom diffusion has been suggested for MgO NCs by GC-MS analysis.[34] From these results, we assign the −17.7 ppm resonance to ^{17}O nuclei in the ZnO core and the lower-frequency resonances to ^{17}O nuclei at the surface or in the first sublayers of ZnO NCs.

ZnO contains several donor-like defects: oxygen vacancies, interstitial zinc, or hydrogen atoms that lead to different oxygen

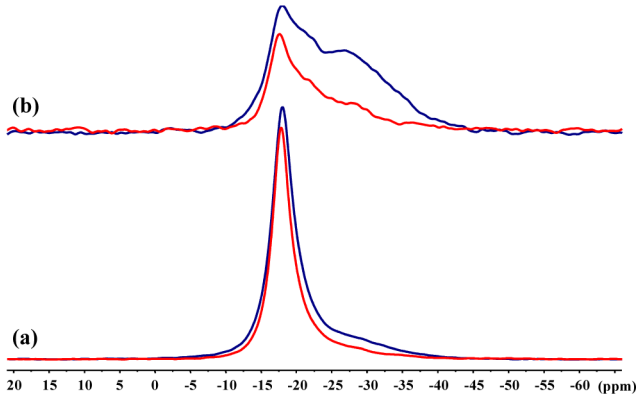

Figure 4. ^{17}O MAS (a) and ^{17}O CP/MAS (b) spectra of vacuum-dried ^{17}O-synthesized isotropic ZnO NCs (sample 1′) before (blue) and after (red) 4 days exposure to unenriched water.

surroundings in the material. Hydroxyl groups can also exist at the surface of the NCs. Each of these O surroundings will lead to a signal with a specific chemical shift. An assignment of the different ^{17}O resonances of the ZnO NCs can be suggested. ^{17}O atoms spatially close to ^{1}H atoms[35] (i.e., surface hydroxyl groups or O atoms close to interstitial H atoms)[14,36] were evidenced by cross-polarization (CP) MAS experiments[37] and T_1 relaxation measurements (vide infra), with shorter ^{17}O relaxation time being expected when O and H atoms are close to each other.[38] ^{17}O CP/MAS performed on sample 1 shows the O atoms close to H atoms that can be exchanged during the contact with water molecules (Figures 5a and S12; see Figure

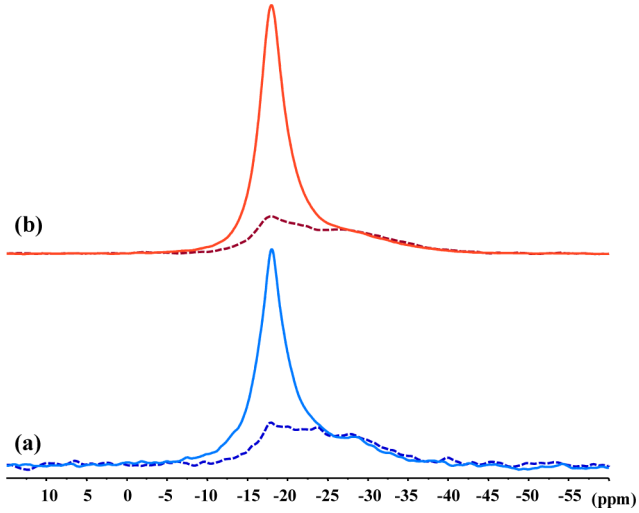

Figure 5. ^{17}O MAS (solid) and ^{17}O CP/MAS (dotted) spectra of vacuum-dried (a) ^{17}O-exchanged isotropic ZnO (sample 1) and (b) ^{17}O-synthesized isotropic ZnO NCs (sample 1′).

S13 for sample 2). In addition, ^{17}O CP/MAS performed on sample 1′ (Figures 5b and S14) shows all the possible O atoms close to H atoms in ZnO NCs. ^{17}O CP/MAS of samples 1 and 1′ look quite similar. Notably, Figure 5a reveals ^{17}O CP/MAS signals at low, medium, and high frequencies as for the standard direct excitation spectrum indicating that O atoms close to H atoms are exchangeable irrespective of their location in the NC. Clearly, the −17.7/lower frequency intensity ratio is much lower in the CP/MAS (ratio of ∼27/73) than in the direct experiment (ratio of ∼80/20). It indicates a higher proportion

DOI: 10.1021/jacs.6b08769
J. Am. Chem. Soc. 2016, 138, 16322−16328

of O and H atoms close to each other for the lowest-frequency resonances. Note that drying the NCs was necessary to record the ^{17}O CP/MAS spectra (Figure S15).[39] However, the magnetization loss of 56(±5)% of the ^{17}O CP/MAS signals of sample 1′ after its exposure to normal water (Figure 4b and S16) states that about half of the O atoms located in proximity of H atoms are not exchangeable. Note that the signal decrease is more important for O-sites detected at low frequencies (losses of 28(±3), 30(±8), and 70(±6)% for the high-, medium-, and low-frequency signals, respectively), strengthening that O atoms located in proximity to H atoms are increasingly numerous from the core to the shell.

Considering the outcome of these experiments, a tentative assignment of the different O resonances may be devised. The high-frequency resonance (i.e., −17.7 ppm) can be confidently attributed to O atoms with Zn−O−Zn bonds mostly located in the core of the NCs. This is the main signal of ^{17}O-enriched ZnO NCs (sample 1′), and it corresponds to the signal previously observed on bulk or big ZnO nanoparticles.[16−18] The low- and medium-frequency signals can be assigned mostly to O atoms in proximity to H atoms on the basis of (i) their stronger signal intensity ratio in the ^{17}O CP/MAS experiments compared to the core signal (−17.4/lower frequencies intensity ratio ∼27/73), while the opposite was found in the ^{17}O experiment with direct excitation (−17.7/lower frequencies intensity ratio ∼80/20) (Figure 5a); (ii) their shorter T_1 relaxation times (i.e., 1.0(±0.2) and 0.8(±0.2) s for −23.5 and −29.4 ppm, respectively) compared to the core resonance one (2.6(±0.1) s). Furthermore, the low- and medium-frequency signals show faster apparent exchange rates in the isotope-exchange experiments ($k_{(med)}$ and $k_{(low)}$, Table 1) than the core signal ($k_{(high)}$). The signal at lowest frequency (i.e., −29.4 ppm) is associated with the fastest apparent exchange rate with H_2O ($k_{(low)}$) and can be assigned to O atoms or hydroxyl groups located at the surface of ZnO. Note that this signal shifts when water molecules are removed by vacuum-drying, suggesting interaction with a water molecule (i.e., through hydrogen bond) and supporting its assignment to O atoms located at the ZnO surface (Figures S15-3). Finally, the medium-frequency resonance (i.e., −23.5 ppm), which exhibits chemical shifts, apparent exchange rate, and T_1 intermediate between that of the high- and low-frequency resonances, can be assigned to O atoms located in the first sublayers of the ZnO NC.

To sum up, the ^{17}O NMR spectrum of the ^{17}O-exchanged ZnO NCs consists of resonances of core O atoms (−17.7 ppm), surface O atoms and hydroxyl groups (−29.4 ppm), and O atoms from the first sublayers (−23.5 ppm, Figure 6). These resonances are characteristic of different surroundings of the O atoms that are undoubtedly related to defects of ZnO NCs. The ^{17}O low-frequency signals at −23.5 and −29.4 ppm are observed for the first time thanks to both the in situ procedure that favored the observation of surface sites and the small size of the ZnO NCs. Indeed, in the case of isotropic NCs of 5.6 nm, the total amount of O atoms present at the surface of ZnO NCs is ca. 21%, while it is only ca. 7% of the total oxygen atoms of 15 nm ZnO NCs. The signal corresponding to these surface atoms should be therefore weaker for large NCs or bulk ZnO. This explains probably why the ^{17}O ZnO surface signals were not observed in the few previous ^{17}O spectra of ZnO.[16−18] The difference between the chemical shifts of the signals associated with the ^{17}O atoms in the core and the ones located close to or at the surface is small compared to the differences observed for other materials (e.g., Ce_2O_3 and SiO_2).[8−11,22,40] This is probably related to the high ionicity of the Zn−oxygen bond.[8] Density functional theory (DFT) calculations could help to support these assignments.

The ^{17}O-exchange experiments also suggest that the atoms of ZnO NC are neither fixed nor frozen, and changes over successive contact with water can thus be explored. ^{17}O MAS NMR experiments performed on sample 1 after it reached the equilibrium state (step 1), followed by a vacuum-drying period, a subsequent exposure for >12 h to standard H_2O, and a final vacuum-drying period (step 2) (Figure S17), revealed notable residual ^{17}O signals of ∼30% of the initial signal (i.e., at step 1). Obviously, part of the ^{17}O atoms are irreversibly incorporated into the ZnO NCs while a larger fraction remains exchangeable. The incidence of the watering/drying cycles on global ^{17}O apparent exchange rates was investigated on isotropic ZnO NCs after two (sample 3) or six (sample 4) cycles of long exposure to water (>12 h) followed by vacuum-drying at room temperature (Figure 7 and Figures S18 and S19).

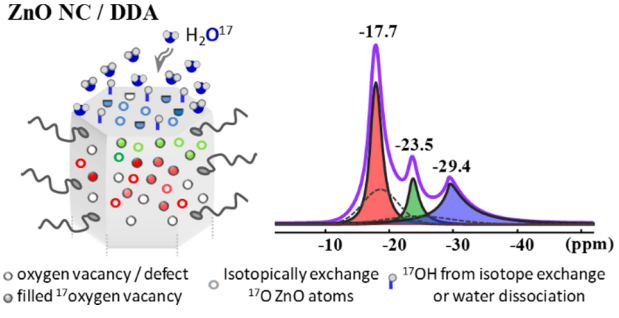

Figure 6. Schematic view of the different oxygen atoms in ZnO NCs.

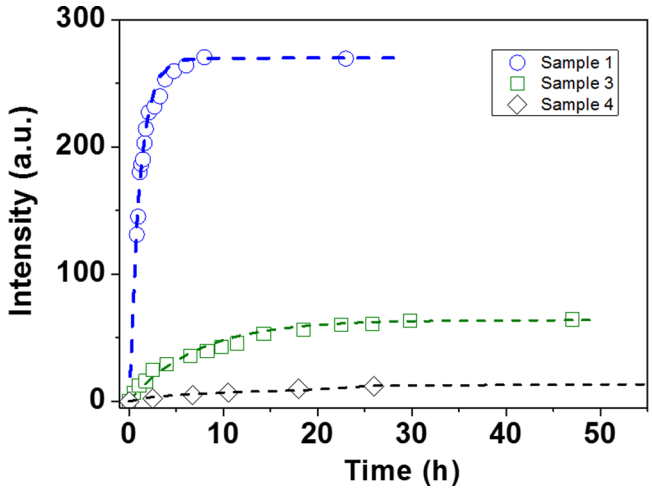

Figure 7. Global ^{17}O signal intensities of sample 1 (blue ○), sample 3 (green □), and sample 4 (gray ◊) as a function of exposure time to H_2O enriched in ^{17}O. The fitting curves are represented by the dashed lines (---) using the equation $I(t) = I(\infty)[1 - \exp\{-k \cdot t\}]$.

Both samples 3 and 4 revealed reduced global isotope apparent exchange rate with $k_{glo} \approx 0.14$ and 0.06 h^{-1}, respectively, and much smaller IEL (64 and 15, respectively) than sample 1 (Table 1 and Figure S20). The numbers of watering/drying cycles clearly diminish the propensity of the ZnO NC for exchanging O atoms with H_2O. Several reasons can be invoked to account for these observations. Water

DOI: 10.1021/jacs.6b08769
J. Am. Chem. Soc. 2016, 138, 16322−16328

dissociation rate might be reduced because of a surface reconstruction, as reported by Abriou and Jupille for MgO surfaces.[41] This surface reconstruction may involve migration of defects from the core to the surface of the NCs during the watering/drying cycles. As the number of cycles increases, the core defects lessen, making more difficult an exchange of core O atoms. This hypothesis is supported by the evolution of the relative contribution of the high-frequency resonance (i.e., −17.7 ppm) observed in the 1D T_1-filtered ^{17}O MAS spectra of the isotropic NCs. The −17.7 ppm resonance ratio (82%, 61%, and 28% for samples 1, 3, and 4, respectively) strongly decreases after, respectively, two (sample 3) and six (sample 4) watering/drying cycles with respect to sample 1 (Table 1). The lesser insertion of ^{17}O in the core of the NCs emphasizes that the structural evolution involves not only surface atoms but also deeper layers of the ZnO particles. These results are in line with theoretical studies reporting that O vacancies prefer to be located at surface sites of ZnO and have lower migration barriers for moving from the central region toward the surface of a wire rather than from surface to internal sites.[42] The migration of the interstitial O atoms by the kick-out mechanism leading to the self-diffusion of O atoms for n-type ZnO is expected to take place down to a very low temperature and can diffuse efficiently.[42] It may be noticed that k_{glo} is dramatically different for samples 1 and 3 (0.88 and 0.14 h^{-1}, respectively) while it is much closer for samples 3 and 4 (0.14 and 0.06 h^{-1}, respectively). As mentioned above, several phenomena contribute to k_{glo}. The larger value found for sample 1 may be related to the first contact of ZnO NC with H_2O, resulting in the first hydroxylation of the surface of the sample, in addition to the other processes that also take place for samples 3 and 4.

The structural evolution deep inside the NCs evidenced by NMR spectroscopy is supported by powder X-ray diffraction data. Figure 8 shows the XRD patterns of samples 1, 3, and 4.

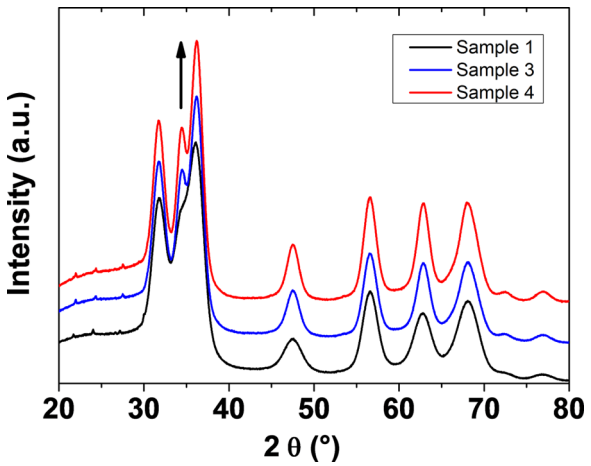

Figure 8. X-ray powder diffraction patterns of isotropic ZnO NCs sample 1 just after synthesis after two watering/drying cycles (sample 3) and after six watering/drying cycles (sample 4).

Regardless of the peak, the coherence length of the NCs increases from sample 1 to sample 4, while the size of the NCs remains similar, thus confirming the better crystallinity of the sample after the watering/drying cycles (Figure S21). This is in agreement with the global decreases of the apparent exchange rates with the increased number of water exposure cycles that can be associated with a diminution of the number of ZnO defects. The presence (or absence) of such defects is of tremendous importance for applications. Specific applications will necessitate their presence, while for others defects should be avoided. For example, in catalysis or gas-sensor applications, a decrease of the performances is usually observed in the presence of water.[43] Our study shows that this performance decay is consistent with the defects having been removed and that one must minimize as much as possible the basal faces in order to keep the defects as long as possible. Consequently, the use of anisotropic NCs can meet this need. On the other hand, for optic or optoelectronic application, defect-free NCs are required.[44] The proposed water-drying treatment is advantageous as it should allow one to remove defects while keeping the nanosize and colloidal properties of the NCs, properties that are usually appreciably altered using standard thermal treatment.

CONCLUSION

The gathered results have shown that ^{17}O MAS NMR spectroscopy is a very convenient, efficient, and powerful technique to trace exchange and core dynamics of metal oxide NCs. This allowed proof for the first time of a dynamic behavior of the O atoms in NCs of ZnO. These take place not only at the surface of the NCs but also inside the core. These investigations also revealed that a soft postsynthesis process consisting of watering/drying cycles leads to more crystalline and static structure, suggesting that such a postsynthesis process may greatly improve long-term stability of metal oxide NCs.

EXPERIMENTAL SECTION

Solid-State NMR Experiments. Solid-state NMR experiments were recorded at 300 K on a Bruker AvanceIII spectrometer operating at 9.4 T. Samples were packed into 3.2 mm zirconia rotors inside a glovebox. The rotors were spun at 10 kHz at room temperature. For ^{17}O MAS single-pulse experiments, small flip angle ($\pi/6$) pulses were used with recycle delay of 10 s. 1D T_1-filtered ^{17}O MAS were acquired with a 1D NOESY experiment pulse program where the delays where synchronized with the spinning rate. The experiment consists of two consecutive ^{17}O 90° pulses separated by one spinning period followed by a time delay t_{filter} of 40 ms and then another ^{17}O 90° before detection to suppress ^{17}O signals with spin−lattice relaxation times T_1 shorter than the delay t_{filter}. The 1D T_1-filtered ^{17}O MAS were performed with a recycle time of 2 s to follow the isotope-exchange kinetics and one of 20 s for quantification purposes (relative population and isotopic enrichment level). ^{17}O CP/MAS spectra were recorded with a recycle delay of 3 s and a contact time of 5 ms. Spin-lock radiofrequency fields were set for ^{1}H and ^{17}O nuclei to 57 and 47 kHz, respectively. ^{17}O relaxation times T_1 were measured with the saturation-recovery or inversion-recovery methods. Chemical shifts were referenced to liquid water at 0 ppm. Spectra were fitted using the DMfit software.[45] The central transition was modeled by the Czjzek model with the d parameter set to 5. Spinning sidebands of satellite transitions were simulated using Lorentzian/Gaussian lineshapes.

Synthesis. All reactions were carried out under water- and oxygen-free argon atmosphere using standard Schlenk tubes and glovebox techniques. Tetrahydrofuran (THF) was dried using an MBraun SPS column. The residual water contents of the solvent were systematically measured by Karl Fischer coulometric titration by using Metrohm equipment. $[Zn(C_6H_{11})_2]$ was purchased from NanoMeps and used as received.[46] Dodecylamine (DDA) was purchased from Aldrich and used as received. H_2O was distilled under argon and degassed by bubbling argon for 30 min. H_2O-enriched in ^{17}O (20% ^{17}O) was purchased from Euriso-top and degassed by bubbling argon for at least 30 min.

DOI: 10.1021/jacs.6b08769
J. Am. Chem. Soc. 2016, 138, 16322−16328

Preparation of Isotropic NCs (Sample 1). In a dry Schlenk tube, $[Zn(C_6H_{11})_2]$ (231.7 mg, 1 mmol) and DDA (185.4 mg, 1 equiv, 1 mmol) were dissolved in 12 mL of THF and vigorously stirred at room temperature for 5 min protected from light. THF (0.47 mL) containing H_2O (2 equiv, 2 mmol) was then added dropwise to the $[Zn(C_6H_{11})_2]$ and DDA mixture. After 16 h, the solvent was removed under vacuum to quantitatively yield isotropic ZnO NCs.

Washing Procedure. Acetone (10 mL, previously dried over activated molecular sieves and stored in the glove box) was added to the THF solution of isotropic ZnO NCs, and the mixture was centrifugated at 5000 rotations per minute (rpm) for 5 min. After removal of the supernatant, the operation was repeated 3 times and the white suspension was dried under vacuum for 6 h.

Preparation of Sample for NMR Experiments. Washed isotropic ZnO NCs (30 mg) were placed in zirconia rotor for solid-state NMR experiments.

Addition of H_2O Enriched in ^{17}O. Under argon, 20 μL of degassed H_2O enriched with ^{17}O (20% ^{17}O) was added directly inside the zirconia rotor containing 30 mg of isotropic ZnO NCs, and solid-state NMR experiments were recorded.

Preparation of Nanorods (Sample 2). In a two-necked reactor, $[Zn(C_6H_{11})_2]$ (231.7 mg, 1 mmol) and DDA (370.7 mg, 2 equiv, 2 mmol) were mixed in a vial under argon protected from light. When a viscous solution was formed, 72 μL of H_2O (4 equiv, 4 mmol) was then carefully added inside the two-necked reactor with careful precaution taken to avoid contact of the water droplet with the $[Zn(C_6H_{11})_2]$ and DDA mixture. Slow diffusion of water vapors for 4 days allowed the quantitative formation of ZnO nanorods. The washing procedure in air, the preparation of the sample for NMR experiments, and the addition of H_2O enriched in ^{17}O were performed as described above.

Preparation of Isotropic ZnO Enriched in ^{17}O. The synthesis of isotropic ZnO enriched in ^{17}O was performed in a similar manner as for the synthesis of isotropic ZnO NCs (preparation of sample 1), but this time using H_2O enriched in ^{17}O instead of unenriched H_2O and 0.2 equiv of DDA.

Transmission Electron Microscopy. Samples for transmission electron microscopy (TEM) analysis were prepared by slow evaporation of droplets of colloidal THF solution deposited on carbon-supported copper grids. The samples were dried overnight under vacuum (1×10^{-5} mbar) by using a BOC Edward turbomolecular pump. The TEM experiments were recorded at the "Service Commun de Microscopies de l'Université Paul Sabatier" TEMSCAN on a JEOL JEM1011 electron microscope operating at 100 kV. The nanoparticle size-distribution histograms were determined by using magnified TEM images. The size distributions of the isotropic (sample 1) and nanorod (sample 2) NCs were determined by measuring a minimum of 500 particles for each sample. The mean diameter was evaluated by fitting of the histogram with a Gaussian curve. The first value corresponds to the center of the peak, whereas the second one corresponds to twice the standard deviation of the Gaussian distribution or ~0.849 the width of the peak at half-height (see Figure S2).

Powder X-ray Diffraction. The X-ray powder diffraction patterns have been obtained on a SEIFERT XRD 300 TT diffractometer operated under Cu Ka radiation, fitted with a diffracted beam graphite monochromator. The data have been collected in the 2θ configuration between 10 and 70°. Average crystallite size values (full width at half-maximum) were calculated by Debye−Scherrer formula with PANalytical HighScore Plus program.

■ ASSOCIATED CONTENT

Supporting Information

The Supporting Information is available free of charge on the ACS Publications website at DOI: 10.1021/jacs.6b08769.

Histograms, PXRD patterns, and additional NMR spectra (PDF)

■ AUTHOR INFORMATION

Corresponding Authors

*yannick.coppel@lcc-toulouse.fr

*myrtil.kahn@lcc-toulouse.fr

ORCID

Myrtil L. Kahn: 0000-0003-3079-5759

Notes

The authors declare no competing financial interest.

■ ACKNOWLEDGMENTS

The authors thank L. Vendier from LCC for helpful assistance for XRD. The authors acknowledge the financial support of the Centre National de la Recherche Scientifique (CNRS).

■ REFERENCES

(1) Abenojar, J.; Pantoja, M.; Martínez, M. A.; del Real, J. C. *J. Compos. Mater.* **2015**, *49*, 2963.

(2) Daté, M.; Okumura, M.; Tsubota, S.; Haruta, M. *Angew. Chem., Int. Ed.* **2004**, *43*, 2129.

(3) Baraton, M.-I.; Merhari, L. *J. Eur. Ceram. Soc.* **2004**, *24*, 1399.

(4) Dargatz, B.; Gonzalez-Julian, J.; Guillon, O. *J. Cryst. Growth* **2015**, *419*, 69.

(5) Bonhomme, C.; Gervais, C.; Laurencin, D. *Prog. Nucl. Magn. Reson. Spectrosc.* **2014**, *77*, 1.

(6) Marbella, L.; Millstone, J. *Chem. Mater.* **2015**, *27*, 2721.

(7) Chadwick, A. V.; Poplett, I. J. F.; Maitland, D. T. S.; Smith, M. E. *Chem. Mater.* **1998**, *10*, 864.

(8) Ashbrook, S. E.; Smith, M. E. *Chem. Soc. Rev.* **2006**, *35*, 718.

(9) Shen, L.; Peng, L. *Chin. J. Catal.* **2015**, *36*, 1494.

(10) Sun, X.; Dyballa, M.; Yan, J.; Li, L.; Guan, N.; Hunger, M. *Chem. Phys. Lett.* **2014**, *594*, 34.

(11) Shen, L.; Peng, L. *Chin. J. Catal.* **2015**, *36*, 1494.

(12) Raj, C. C.; Prasanth, R. *J. Power Sources* **2016**, *317*, 120.

(13) Zhang, Q.; Li, H.; Gan, L.; Ma, Y.; Golberg, D.; Zhai, T. *Chem. Soc. Rev.* **2016**, *45*, 2694.

(14) Wang, Z. L.; Wu, W. *Natl. Sci. Rev.* **2014**, *1*, 62.

(15) Arya, S. K.; Saha, S.; Ramirez-Vick, J. E.; Gupta, V.; Bhansali, S.; Singh, S. P. *Anal. Chim. Acta* **2012**, *737*, 1.

(16) Turner, G. L.; Chung, E. S.; Oldfield, E. *J. Magn. Reson.* **1985**, *64*, 316.

(17) Müller, M.; Hermes, S.; Kähler, K.; van den Berg, M. W. E.; Muhler, M.; Fischer, R. A. *Chem. Mater.* **2008**, *20*, 4576.

(18) Wang, M.; Yu, G.; Ji, W.; Li, L.; Ding, W.; Peng, L. *Chem. Phys. Lett.* **2015**, *627*, 7.

(19) Meyer, B.; Rabaa, H.; Marx, D. *Phys. Chem. Chem. Phys.* **2006**, *8*, 1513.

(20) Raymand, D.; van Duin, A. C. T.; Spångberg, D.; Goddard, W. A., III; Hermansson, K. *Surf. Sci.* **2010**, *604*, 741.

(21) Kunat, M.; Girol, St. G.; Burghaus, U.; Wöll, Ch. *J. Phys. Chem. B* **2003**, *107*, 14350.

(22) Wang, Y.; Muhler, M.; Wöll, Ch. *Phys. Chem. Chem. Phys.* **2006**, *8*, 1521.

(23) Kahn, M. L.; Glaria, A.; Pages, C.; Monge, M.; Saint Macary, L.; Maisonnat, A.; Chaudret, B. *J. Mater. Chem.* **2009**, *19*, 4044.

(24) Glaria, A.; Kahn, M. L.; Cardinal, T.; Senocq, F.; Jubera, V.; Chaudret, B. *New J. Chem.* **2008**, *32*, 662.

(25) Chassaing, P.-M.; Demangeot, F.; Paillard, V.; Zwick, A.; Combe, N.; Pagès, C.; Kahn, M. L.; Maisonnat, A.; Chaudret, B. *Appl. Phys. Lett.* **2007**, *91*, 053108.

(26) Chassaing, P.-M.; Demangeot, F.; Combe, N.; Saint Macary, L.; Kahn, M. L.; Chaudret, B. *Phys. Rev. B: Condens. Matter Mater. Phys.* **2009**, *79*, 155314.

(27) d'Espinose de Lacaillerie, J. B.; Fretigny, C.; Massiot, D. *J. Magn. Reson.* **2008**, *192*, 244.

(28) Neuville, D. R.; Cormier, L.; Massiot, D. *Geochim. Cosmochim. Acta* **2004**, *68*, 5071.

DOI: 10.1021/jacs.6b08769
J. Am. Chem. Soc. 2016, 138, 16322−16328

(29) Massiot, D.; Messinger, R.; Cadars, S.; Deschamps, M.; Montouillout, V.; Pellerin, N.; Veron, E.; Allix, M.; Florian, P.; Fayon, F. *Acc. Chem. Res.* **2013**, *46*, 1975.
(30) Cadars, S.; Smith, B. J.; Epping, J. D.; Acharya, S.; Belman, N.; Golan, Y.; Chmelka, B. F. *Phys. Rev. Lett.* **2009**, *103*, 136802.
(31) Vasconcelos, F.; Cristol, S.; Paul, J.-F.; Delevoye, L.; Mauri, F.; Charpentier, T.; Le Caër, G. *J. Phys.: Condens. Matter* **2013**, *25*, 255402.
(32) Massiot, D.; Bessada, C.; Coutures, J. P.; Taulelle, F. *J. Magn. Reson.* **1990**, *90*, 231.
(33) Ernst, H.; Freude, D.; Mildner, T.; Pfeifer, H. In *Proceedings of the 12th International Zeolite Conference*; Treacy, M. M. J., Marcus, B. K., Bisher, M. E., Higgins, J. B., Eds.; Materials Research Society, Warrendale, PA, 1999; p 2955.
(34) Li, Y.; Klabunde, K. *Chem. Mater.* **1992**, *4*, 611.
(35) Walter, T. H.; Turner, G. L.; Oldfield, E. *J. Magn. Reson.* **1988**, *76*, 106.
(36) (a) Park, J. K.; Lee, K. W.; Lee, C. E. *Appl. Phys. Lett.* **2013**, *103*, 023109. (b) Park, J. K.; Lee, K. W.; Lee, C. E. *Solid State Commun.* **2013**, *165*, 19.
(37) The $^{1}H/^{17}O$ CP/MAS experiment did not increase the overall sensitivity of ^{17}O resonances but allowed for editing O atoms close to H atoms.
(38) van Eck, E. R. H.; Smith, M. E.; Kohn, S. C. *Solid State Nucl. Magn. Reson.* **1999**, *15*, 181.
(39) Wang, M.; Wu, X.-P.; Zheng, S.; Zhao, L.; Li, L.; Shen, L.; Gao, Y.; Xue, N.; Guo, X.; Huang, W.; Gan, Z.; Blanc, F.; Yu, Z.; Ke, X.; Ding, W.; Gong, X.-Q.; Grey, C. P.; Peng, L. *Science Advances* **2015**, *1*, e1400133.
(40) Merle, N.; Trébosc, J.; Baudouin, A.; Rosal, I. D.; Maron, L.; Szeto, K.; Genelot, M.; Mortreux, A.; Taoufik, M.; Delevoye, L.; Gauvin, R. M. *J. Am. Chem. Soc.* **2012**, *134*, 9263.
(41) Abriou, D.; Jupille, J. *Surf. Sci.* **1999**, *430*, L527.
(42) Deng, B.; da Rosa, A. L.; Frauenheim, Th.; Xiao, J. P.; Shi, X. Q.; Zhang, R. Q.; Van Hove, M. A. *Nanoscale* **2014**, *6*, 11882.
(43) (a) Rapson, T. D.; Dacres, H. *TrAC, Trends Anal. Chem.* **2014**, *54*, 65. (b) Panayotov, D. A.; Morris, J. R. *Surf. Sci. Rep.* **2016**, *71*, 77.
(44) (a) Samokhvalov, P.; Artemyev, M.; Nabiev, I. *Chem. - Eur. J.* **2013**, *19*, 1534. (b) Ledentsov, N. N.; Bimberg, D.; Alferov, Zh. I. *J. Lightwave Technol.* **2008**, *26*, 1540. (c) Wang, N.; Cai, Y.; Zhang, R. Q. *Mater. Sci. Eng., R* **2008**, *60*, 1.
(45) Massiot, D.; Fayon, F.; Capron, M.; King, I.; Le Calvé, S.; Alonso, B.; Durand, J.-O.; Bujoli, B.; Gan, Z.; Hoatson, G. *Magn. Reson. Chem.* **2002**, *40*, 70.
(46) Monge, M.; Kahn, M. L.; Maisonnat, A.; Chaudret, B. *Angew. Chem., Int. Ed.* **2003**, *42*, 5321.

DOI: 10.1021/jacs.6b08769
J. Am. Chem. Soc. 2016, 138, 16322−16328